Journal of Colloid and Interface Science 344 (2010) 1–9

Contents lists available at ScienceDirect

Journal of Colloid and Interface Science

www.elsevier.com/locate/jcis

Templated one step electrodeposition of high aspect ratio *n*-type ZnO nanowire arrays

Satinder K. Sharma, Amritha Rammohan, Ashutosh Sharma *

DST Unit on Nanosciences and Department of Chemical Engineering, Indian Institute of Technology, Kanpur, India

ARTICLE INFO

Article history:
Received 5 August 2009
Accepted 12 December 2009
Available online 21 December 2009

Keywords:
ZnO nanowire
Aligned nanowire
Electrochemical synthesis
Templated synthesis
Nanowire growth kinetics
n-Type nanowire
Hot-Probe
Nanowire characterization
μ-Raman

ABSTRACT

High aspect ratio Zinc Oxide (ZnO) nanowires (NWs) were synthesized by template based one-step electrochemical deposition (OSECD) technique. The electro-reduction of hydroxide ions in the presence of Zn^{2+} ions within $Zn(NO_3)_2$ is involved in the growth of ultra thin NWs arrays. Field Emission Scanning Electron Microscopy (FESEM) images revealed that the growth rates of different crystal faces, (0 0 0 1) and $(000\bar{1})$, were different at different deposition potential for the high aspect ratios ZnO NWs arrays. The *n*-type semiconductor conductivity of ZnO NWs was ascertained by a Hot-Probe approach. X-ray diffraction results demonstrated that the grown ZnO NWs had wurtzite crystal structure with unit cell parameters $a = 2.93$ Å, $c = 5.45$ Å and a deterioration of preferred (1 0 1) orientation is observed at more negative deposition potentials. Small angle X-ray scattering (SAXS) results evidenced that the NW arrays grown at −1.2 V have higher fraction of larger crystallites. Micro-Raman spectroscopy analysis showed that the variation in E_2 (high) vibration mode at 435 cm^{-1} is coupled with an increase in electro acceptor oxygen atoms incorporated within ZnO NWs at −1.2 V.

1. Introduction

Recently, one dimensional nanostructures have attracted tremendous interest because of their technological potential. In particular, Zinc Oxide nanowires/nanorods and thin films are receiving intense interest, due to their extensive applications in a number of fields such as chemical sensors, gas sensors, optoelectronic devices, resonators, piezoelectric transducers, light emitting devices, photosensors, Al/Au Ohmic contacts, direct band gap semiconductors and wireless devices with self powering capability [1–5]. The major challenges for process engineers are to reproducibly grow aligned, high aspect ratio, *n*-type ZnO nanostructures, control their resistivity and measure the nature (electrons or holes) of charge carriers within the structures. Non-aligned *n*-type ZnO nanostructures can be grown by appropriate doping in conjunction with the techniques such as high temperature vapor phase methods, RF Magnetron sputtering, MOCVD, pulsed-laser ablation, microwave, hydrothermal and sol–gel [6–12]. Electrochemical deposition is another simple technique which has been explored to grow ZnO nanowire structures [13–15]. Peulon and Lincot [16] demonstrated the solution based deposition of ZnO films from $ZnCl_2$ salt in the presence of supporting electrolyte KCl and dissolved oxygen as a precursor. The influence of precursor concentration, pH, temperature and properties of the films were investigated by several techniques [16].

Izaki and Omi as well as Shinagawa et al., presented the deposition of Zinc Oxide thin films from 0.1 M Zinc nitrate solution kept at 335 K and observed the increase in concentration of OH^- ions at the electrode [17,18]. The synthesis of nanostructures by electroreduction has allowed the reproducible and affordable fabrication of such nanometric regime structures. The focus is especially on the field of printed electronics since they are two to three orders of magnitude cheaper per unit area than conventional semiconductor manufacturing. However, most of the present printable semiconductors suffer from poor air-stability, complicated packaging, degraded device lifetime and toxic nature of organics and chalcogenides, etc. Therefore, *n*-type ZnO nanostructure is a possible alternative because of its soluble nature, optical transparency and it can be easily implemented with the existing processing technology [19]. The template based synthesis of nanostructures in a membrane is an elegant chemical approach for the fabrication of aligned nanowires/nanotubes with a good control over their diameter and aspect ratio. Zheng et al. [20] proposed the anodic alumina membrane (AAM) based one-step electrochemical deposition technique for ZnO nanowire growth. These single crystal nanowires were grown by three probe DC method in 0.1 M $ZnNO_3$ solution at 343 K and 1 V potential and characterized by PL measurements (400–750 nm). Lai and Riley [21] synthesized the ZnO nanorods from Zinc ion and either nitrate ions [$ZnNO_3$ (0.01 M)] or hydrogen peroxide as the hydroxide precursors. These, when reduced, result

* Corresponding author. Fax: +91 512 259 0104.
E-mail address: ashutos@iitk.ac.in (A. Sharma).

0021-9797/$ - see front matter © 2009 Elsevier Inc. All rights reserved.
doi:10.1016/j.jcis.2009.12.026

in a local pH change at the electrode interface and the precipitation of ZnO through porous polycarbonate membrane. Polycrystalline nanowires were deposited from the peroxide electrolyte at fixed potential of −0.2 V at 22 °C, while single crystals were grown using nitrate ions at constant potential of −0.7 V at 90 °C. The direction of nanorods grown at the higher temperature is perpendicular to the $(1\,0\,\bar{1}\,1)$ plane. A recent work by Cui [22] investigated the effect of growth time, electrical potential, temperature and templated substrate on the morphology and composition of ZnO nanostructures synthesised by electrochemical deposition from an aqueous solution of Zinc nitrate and hexamine on a seeded Si substrate at the temperatures between 90–95 °C. The SEM images and XRD results show that the effect of negative potential enhanced the growth of single crystalline ZnO nanowires while positive potential results in nanodisks of ZnO and ZnO_2 composite. The growth rate of nanowires was observed to be similar for patterned as well as bare substrates [22]. Among the studies that specifically address field emission properties, Pauporte and Lincot [23] reported the high aspect ratio ~8 of ZnO nanorods, grown at the GaN surface by (0.1 mM) $ZnCl_2$ at 80 °C. Lee et al. [24] studied the field emission property of ZnO nanowires grown at Co nanoparticles dispersed on Si substrates by thermal heating of ZnO powder at 550 °C. The average length, diameter and aspect ratio of fabricated nanowires were 13 μm, 50 nm and 250, respectively. It is clear that the chemical composition, concentration of the reacting species, electrolyte temperature, agitation conditions, pH and additives are parametric knobs that influence the properties, stoichiometry and aspect ratio of the grown nanostructures [6,7,9,13–24]. However, the nature of carrier (*n*- or *p*-type) in the ZnO nanostructures and crystal faces responsible for the growth of aligned high aspect ratio nanowires by electrodeposition in a template have not yet been determined. Further, particle size measurements in ZnO crystallites and variation of acceptor oxygen atom incorporation with the ZnO lattice thus grown have not been performed, which are important in determination of the nanowire tip sharpness that controls field emission property.

The present study aims at the synthesis of high aspect ratio bundle of aligned ZnO nanowires in a polycarbonate membrane by a one-step electrochemical deposition (OSECD) from a dilute Zinc nitrate electrolyte. Effect of deposition potential on the kinetics of wire growth and aspect ratio are studied, which also suggests a mechanism of the nanowires formation and contribution of specific crystal faces for the well aligned growth. The ZnO nanowires grown by this technique are characterized for the type of majority charge carriers, size of crystallites, orientation of crystal planes, faces of crystal and the degree of incorporation of acceptor oxygen atoms within them.

2. Materials and methods

2.1. Synthesis of aligned ZnO nanowires

A typical synthesis of ZnO nano wires were carried out by Auto Lab PGSTAT Model302 (potentiostat/galvanostat) which involves a three-electrode cell system. A platinum strip (99.99% purity; 1.45 cm^2) served as the anode. A saturated silver/silver chloride (Ag/AgCl in saturated KCl) electrode was used as the reference and connected via a salt bridge. (All potentials are reported w.r.t. the potential of reference electrode). Cyclic voltammetry measurements were collected at a scanning speed of 20 mV/min. The average pore size, pore density and thickness of polycarbonate membrane (commercially available Whatman) used as template for the synthesis of ZnO nanowires were 100 nm, 6×10^8 pores/cm^2 and 2 μm, respectively. All the reagents used were RA grade. The electrolyte used for ZnO nanowires fabrication was 0.1 M, $Zn(NO_3)_2{\cdot}6H_2O$ (2.978 gm in 100 ml H_2O) dissolved in Milli-Q ~18 MΩ water. Copper tape served as the cathode substrate for the nanowires' growth. The electrodeposition was carried out at −1.2 V, −1.0 V and −0.8 V, at 75 °C. During deposition the current as a function of time is measured. After electrodeposition the electrolyte was drained out and the polycarbonate membrane was dissolved with choloroform. After that, the samples were subjected to rinsing with water and ethanol.

2.2. Characterization techniques

Field Emission Scanning Electron Microscopy (FESEM) images of grown nanowires were captured using a Carl Zeiss Supra 40 microscope at an acceleration voltage of 10 kV. The atomic percentages or chemical analysis of Zinc and Oxygen in the grown ZnO nanowires were computed by Carl Zeiss FESEM equipped with Oxford Inca energy dispersive X-ray detector, which can access energy range down to 1 keV with its ultra thin window. This feature enables the sensitivity of Energy Dispersive Analysis of X-Rays (EDAX) detector for light elements.

The Hot-Probe analysis of ZnO nanowires was carried out by two 12 mm apart, submicron platinum electrodes. These electrodes were wired with a digital voltmeter to form a close loop circuit. A soldering iron attached with a sharp tungsten tip was used as a heating probe to perform this experiment. The Hot-Probe is connected to the positive terminal of the meter while the cold probe is connected to the negative terminal. Then, the hot electrode was heated up to the required temperature and pinned to the sample surface. All measurements were recorded for 40–60 s approximately.

Thin film X-ray diffraction (XRD) spectra of ZnO nanowires were taken perpendicular to the growth direction on a Thermo Electron diffractometer operating in the θ–2θ Bragg configuration using Cu Kα radiation. Data were collected at a scan rate of $0.075\theta\ min^{-1}$ and sampling interval of 0.002θ. The voltage was set at 45 kV with a 44 mA flux.

The small angle X-ray scattering (SAXS) experiments of ZnO nanowires were performed with HECUS SAWAX (Cu-target, wavelength $\lambda = 0.154$ nm) operating at power of 2 kW. Scattering spectra were monitored in q-range ($q = 4\Pi(\sin\theta)/\lambda$) with 2θ being scattering angle.

The structural analysis of ZnO nanowires was carried out by the WiTec CRM 200 micro-Raman spectrometer coupled with a high resolution confocal optical microscope. The laser excitation of 514.5 nm was provided by an argon laser. The microscope objective used was Nikon 100X, with a working distance of 0.26. All the measurements were made at room temperature, to avoid heating effects in the spectra.

3. Results and discussion

3.1. Chronoamperometry growth kinetics of aligned ZnO NWs

Fig. 1 shows voltammetric curve of the $Zn(NO_3)_2{\cdot}6H_2O$ electrolyte which was utilized for ZnO nanostructure deposition. According to this curve, the process of ZnO formation inside the polycarbonate pores initially involves diffusion of hydroxide ions and Zn^{2+} ions from bulk towards the pore mouth. After that, the ions diffuse towards the bottom of pores and get reduced on the surface of copper tape. The hydroxide ions are immediately precipitated in presence of Zn^{2+} to form $Zn(OH)_2$ which gets easily dehydrated at 75 °C to form ZnO NWs. The phenomenology of the mechanism of this process is shown in inset of Fig. 1. It describes the concentration profile variation inside a single pore after the application of the deposition potential to the electrolyte.

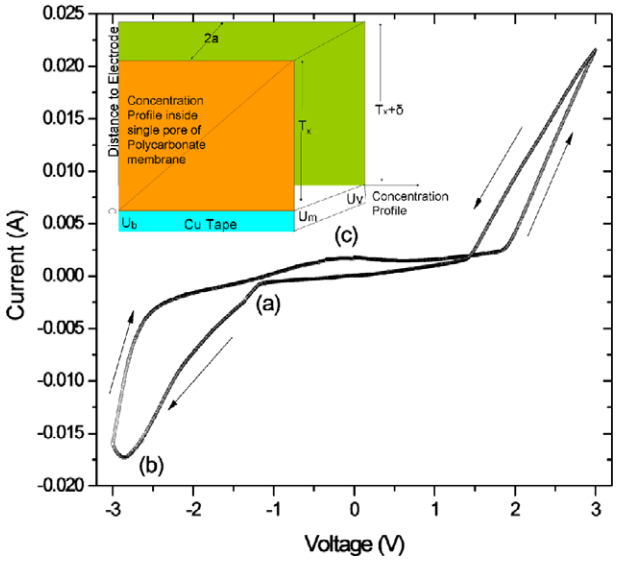

Fig. 1. Cyclic voltammetric curve of $Zn(NO_3)6H_2O$ (cathode, scan rate 20 mV/s, at 75 °C). Inset shows the concentration profile of grown species inside polycarbonate membrane of thickness (T_x), radius (a) and diffusion layer length outside the pores ($T_{x+\delta}$).

The concentrations of the electroactive species in the bottom of the pore, mouth of the pore and the bulk of the solution correspond to U_b, U_m and U_v, respectively [25]. However, in this process, it is not expected that a diffusion layer develops outside the polycarbonate pores. *I–V* characteristics (Fig. 1) show the deposition of Zinc oxide, Zinc and hydroxide ions at (a, b and c respectively) at various potentials. Zinc oxide deposition is associated with a cathodic current below −1.2 V and the reverse potential hysteresis is attributed to the nucleation over potential. However, the electroreduction of nitrate ions to nitrite ions generates hydroxide ions at the cathode. It gives rise to the diffusion controlled reduction wave towards more negative potential [13,26]. The potential at zero current is about −0.2 V which is close to the expected value for a Zn^{2+}/Zn redox system [14]. The steep increase in cathodic current at −1.3 V corresponds to Zinc deposition. During the reverse sweep the deposited zinc starts reoxidizing from −0.2 V. These results indicate a potential window between −0.2 V and −1.2 V for deposition of ZnO. We mostly investigated nanowires grown at −0.8, −1.0 and −1.2 V. High negative potentials (as shown in cyclic voltammetric curve; Fig. 1) at ∼−3 V result in hydrogen evolution and porosity of nanostructures.

A tentative scheme of electroprecipitation of ZnO nanowires from Zinc nitrate solution is given in the following equations

$$NO_3^- + H_2O + 2e^- \rightarrow NO_2^- + 2OH^- \quad (1)$$

$$Zn^{2+} + 2OH^- \rightarrow Zn(OH)_2 \rightarrow ZnO + H_2O \quad (2)$$

$$Zn^{2+} + NO_3^- + 2e^- \rightarrow ZnO + NO_2^- \quad (3)$$

The Zinc ions precipitate with the hydroxyl anions forming Zinc hydroxide which spontaneously dehydrates into ZnO as shown in Eq. (2). The overall mechanism of ZnO deposition from the electrolyte is given in Eq. (3). It may be noted that the electrochemical reduction of nitrate in the electrolyte demands the presence of Zn^{2+} ions in the solution. Postels et al. have proposed a similar mechanism of reduction of nitrate ions to nitrite ions to describe the mechanism of ZnO nanorod deposition [27]. In this work, the deposition of nanorods was accomplished by hindering the rate of Zn^{2+} ions at the substrate by means of a directing agent. Consequently, it has been suggested that the rate of ZnO NWs growth in the nitrate solution is limited by the charge transfer kinetics within the electrolyte.

Therefore, in view of this mechanism, the probability of ZnO nanowires growth without any additive with electroless technique is ruled out. The electroless deposition is only possible by three fundamental mechanisms of reacting species such as autocatalytic, substrate catalyzed, and galvanic displacement, which is not possible in this case [26].

In this study, ZnO nanowires were synthesized by using the chronoamperometry method (constant voltage). The other experimental parameters were carefully controlled and kept constant, except the deposition time.

In order to follow the deposition process, the current was recorded as a function of time. Typically, we can delineate the deposition process into four different zones as shown in Fig. 2 [28]. After immersing the sample in the electrolyte, no external voltage is applied for 10 s until the open-circuit voltage between cathode and anode is stabilized. The voltage is then applied and the current exhibits a sharp increase in the region (I) that is ascribed to the charge in the electrical double layer. Following this, the reduction of Zn^{2+} ions located immediately at the cathode surface occurs. It creates a concentration gradient that causes a flux of ions towards the cathode. In this process, a decrease in current indicates the formation of the diffusion layer on the surface. During the growth of the ZnO needles in the pores, the current remains nearly constant in region (II). Once the ZnO nanowires reach the polymer surface caps start to grow on top of the nanowires. It results in an increase in current in region (III) because of increase in surface area. As shown in Fig. 3A–C current–time (*I–t*) characteristics recorded at different voltages reveal three distinct zones. The current–time characteristics are measured at applied potentials of −1.2 V, −1.0 V and −0.8 V. The slight increase in current at the beginning of deposition indicates the filling of the pores. When all the pores are filled, deposition occurs over the entire surface of the polycarbonate membrane and the current increases abruptly as shown in Fig. 3A, the variation in current at 400 s reveals that the pore filling rate in region (II) is almost negligible for ZnO nanowires grown at −0.8 V, while in Fig. 3B at −1.0 V the rate has been found to be increased beyond region II. Furthermore, in Fig. 3C at the reduction potential −1.2 V current is found to be saturated, which reflects the completely filled pore. Therefore, the concerted effect of deposition potential, diffusion of reacting species and pore filling rate decides the aspect ratio of grown ZnO nanowire array embedded in polycarbonate template. These results indicate that as the po-

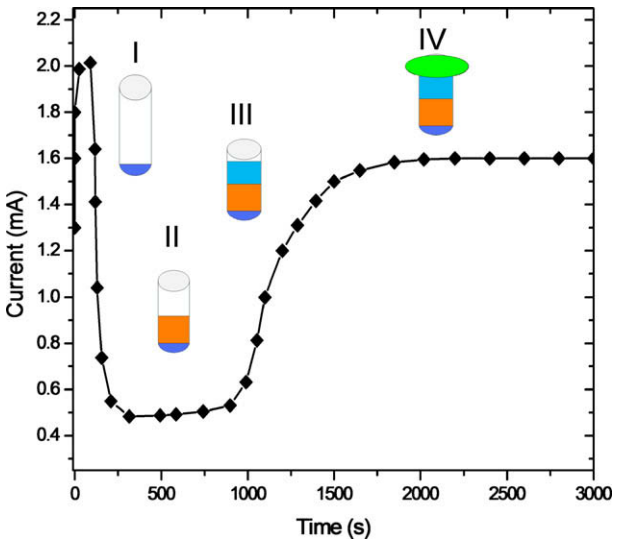

Fig. 2. Typical chronoamperometry (*I–t*) characteristics of template based ZnO nanowire synthesis.

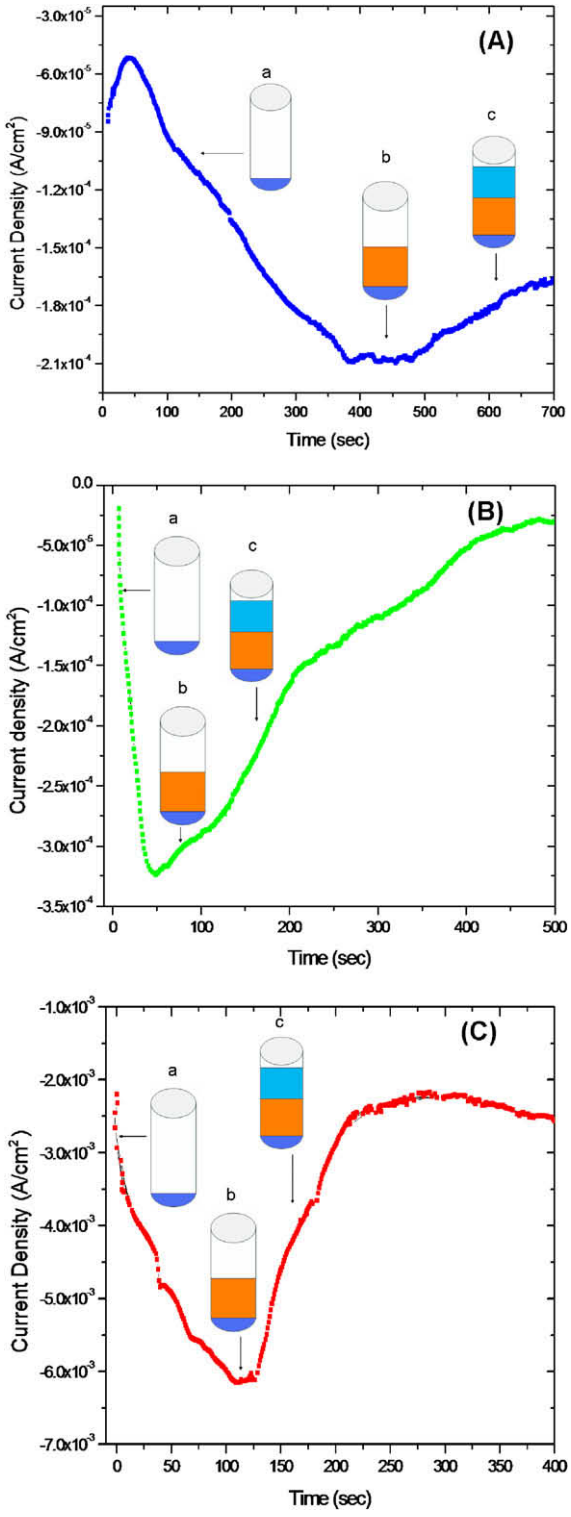

Fig. 3. Current–time (I–t) curve of ZnO nanowires deposition in a polycarbonate membrane with 100 nm diameter of pores at −1.2 V (C), −1.0 V (B) and −0.8 V(A), respectively. The inset shows the different stages of electrodeposition.

tential tends towards the more positive side the transition zone between regions II and III is delayed. This is attributed to the decrease in number of reducible Zn^{2+} ions present in the electrolyte [29], which results in the slow kinetics of pore filling and therefore is a control over the aspect ratio of ZnO nanowires. Izaki and Omi presented an analogous reduction in the deposition rate of Zinc Oxide film with reduction potential [17]. As shown in Fig. 4, ZnO nanowires with well-defined facets are obtained when a potential of −1.2 V is applied to substrate, because of negative potential derives the Zinc ions through the pores of membrane to the surface of substrate and enhances the deposition of ZnO.

Nanowire aspect ratio depends on the nuclei sizes, density and preferential orientation [22]. Only those nuclei with their c-axis perpendicular to the substrate surface can eventually grow into ZnO nanowires spanning across the full thickness of the membrane by diffusion-limited growth. The other nucleation sites with c-axis along the substrate surface or with small inclined angle would stop growing when they are long enough to be blocked by neighboring nanowires. In our case, the membrane thickness was 2 μm, which is also the maximum length of the nanowires obtained. Understanding the kinetics of growth, which is influenced by a host of factors, is important in controlling the wire length before it fills the entire pore.

The morphology of the grown ZnO nanowires was inspected with the help of FESEM as shown in Figs. 4–6. However, the growth rate of the crystal is interconnected to the orientation of the coordination polyhedron at the interface.

Specifically, the crystal face at the corner of the coordination polyhedron present at the interface has the fastest growth rate; the crystal face with the edge of the coordination polyhedron present at the interface has the second fastest growth rate; the crystal face with the face of the coordination polyhedron present at the interface has the slowest growth rate. Therefore, the velocities of crystal growth along different directions have the following relation [30,31]:

$$V_{\langle 0001\rangle} > V_{\langle 01\bar{1}\bar{1}\rangle} > V_{\langle 01\bar{1}0\rangle} > V_{\langle 011\bar{1}\rangle} > V_{\langle 000\bar{1}\rangle} \quad (4)$$

In the coordination structure of the ZnO crystal, the coordination number of Zn is four; all the tetrahedrons are connected together by corner sharing. Fig. 4 shows the morphology of the pyramidal type ZnO nanowires grown by one-step electrochemical technique at −1.2 V have the prismatic form well aligned high aspect ratio nanowires, while the nanowires grown at more positive potential such as −1.0 V and −0.8 V having shortened prismatic form and reduction in high aspect ratio as shown in Figs. 5 and 6.

These results indicate that the growth rates of the (0 0 0 1) and $(000\bar{1})$ faces are different at different deposition potential. For −1.2 V the $(01\bar{1}\bar{1})$ face disappears, while at −1.0 V and −0.8 V $(01\bar{1}1)$ face starts showing their dominating appearance. It leads to the formation of a sharp tip of ~15–20 nm on the grown nanowires. It is clearly seen from the micrographs that the diameter of the wires is approximately similar to the pore size. However, the ZnO nanowires are fragile, and break during the isolation process [32]. The vertical surfaces of the ZnO nanowires shown in Fig. 4 are smooth, suggesting that indicates the walls of the polycarbonate membrane template are also flat.

Fig. 7 shows the variation in the aspect ratio of the grown ZnO nanowires as a function of the deposition potential. The high aspect ratio of ZnO NWs turns out to be higher by a factor of three, as the deposition potential sweeps from −0.8 V to −1.2 V. This implies that at −1.2 V, maximum numbers of Zn^{2+} ions are converted into ZnO nanowires with predominantly longitudinal growth.

The atomic percentage of constituents species from the EDAX measurements were calculated by the intensities of Zn signal normalized for the different samples so that the oxygen signal becomes comparable even at low scattering. No other element was detected in the EDAX spectrum, indicating that the impurities in the samples were below the detection limit of EDAX. The computed atomic percentages of Oxygen and Zinc from EDAX analysis for ZnO NWs grown at the potential −0.8 V, −1.0 V and −1.2 V were 57.4 ± 0.706% and 42.5 ± 0.993%, 60.3 ± 0.317% and

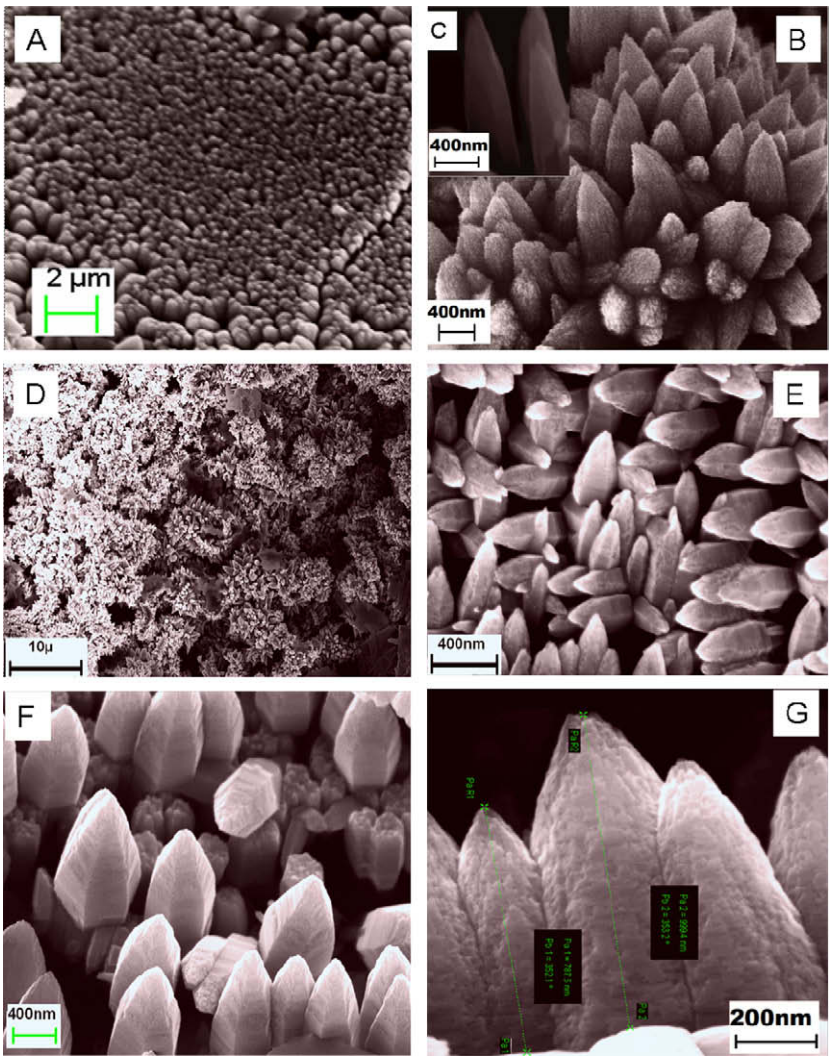

Fig. 4. FESEM micrographs of ZnO nanowires grown from 0.1 M $Zn(NO_3)_2{\cdot}6H_2O$ electrolyte at −1.2 V ((A) aligned NW array, (C) individual nanowires (inset) and (B) cluster of NWs, (D–G) ZnO nanowires at different magnifications).

39.6 ± 0.813% and 79.0 ± 0.625% and 20.9 ± 0.131%, respectively. These results demonstrate the variation in atomic percentage of Zinc and Oxygen as a function of deposition potential. Fig. 8A and B shows the growth mechanism of electrochemically deposited high aspect ratio ZnO nanowires. According to this mechanism, hydroxide ions form at cathode due to electro-reduction of nitrate ions to nitrite ions. It appears to be a major parameter deciding the mode of ZnO growth. Therefore, at −0.8 V crystal $(01\bar{1}\bar{1})$ growth dominating as compared to $(000\bar{1})$, which results the enhancement in lateral direction of ZnO crystal growth and lowest aspect ratio of grown ZnO nanowires as shown in Figs. 6 and 8A. It may be due to at this potential the number of Zn^{2+} ions reacting with hydroxide ions is less, or lack of $Zn(OH)_4^{-2}$, $Zn(OH)^{+}_{(l)}$, $Zn(OH)^{\circ}_{2(l)}$, $Zn(OH)^{-}_{3(l)}$, $Zn(OH)^{2-}_{4(l)}$, etc. complexes in the solution [33,34]. Consequently under the experimental conditions, probability of $Zn(OH)_4^{2-}$ formation was might be higher. As the potential approaches the more negative value (−1.0 V and −1.2 V), the longitudinal growth of ZnO nanowires is higher than the lateral [30,33,34], because of the crystal faces $(01\bar{1}1)$ starts to disappear because of number of $Zn(OH)_4^{-2}$ complex units increasing near the tip where they get adsorbed as shown in Fig. 8B. These Zn^{2+} ions complexes accumulated at the tip and resulted in the (0 0 0 1) face growth of the ZnO crystal. Finally they get reduced in the form of well aligned ZnO nanowire arrays [34]. The nanostructure formed by this mechanism shows high aspect ratio and lattice symmetry as shown in Figs. 4 and 5.

3.2. Majority charge carriers characterization

The estimation of majority charge carriers in the ZnO nanowires is done through Hot-Probe technique. It is a simple yet efficient way to distinguish between *n*-type and *p*-type of ZnO semiconductors nanowires. The ZnO nanowires show a positive voltage 109, 83, 68 mV readout at the voltmeter corresponding to nanowires grown at −1.2 V, −1.0 V and −0.8 V, respectively. This positive magnitude of voltage indicates that grown ZnO nanowires are *n*-type semiconductors. The higher value of readout voltage for −1.2 V shows that the ZnO starts to segregate as a separate phase in the grain boundary regions [35]. A simple explanation for this experiment is that the thermally excited majority free charge carriers are translated within the ZnO nanowires from the Hot-Probe to the cold probe. Thus, the Hot-Probe surrounding zone becomes charged with minority carriers and the cold probe remains neutral [36]. This semiconductor behavior may be a composite effect of oxygen vacancy, Zinc interstitial, Zinc vacancy and interstitial site oxygen within the ZnO nanowires.

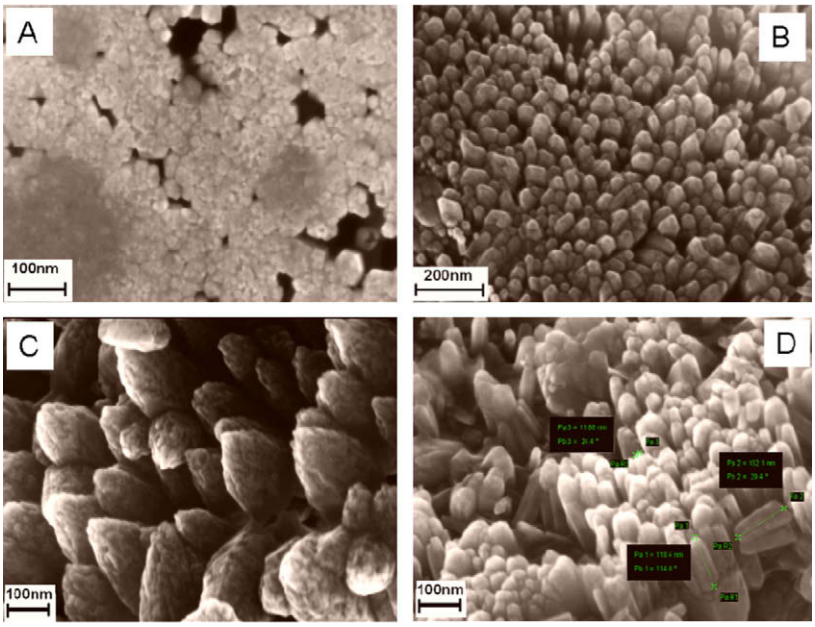

Fig. 5. FESEM micrographs of ZnO nanowires prepared from 0.1 M $Zn(NO_3)_2{\cdot}6H_2O$ electrolyte at −1.0 V ((A–D) ZnO nanowires at different magnifications).

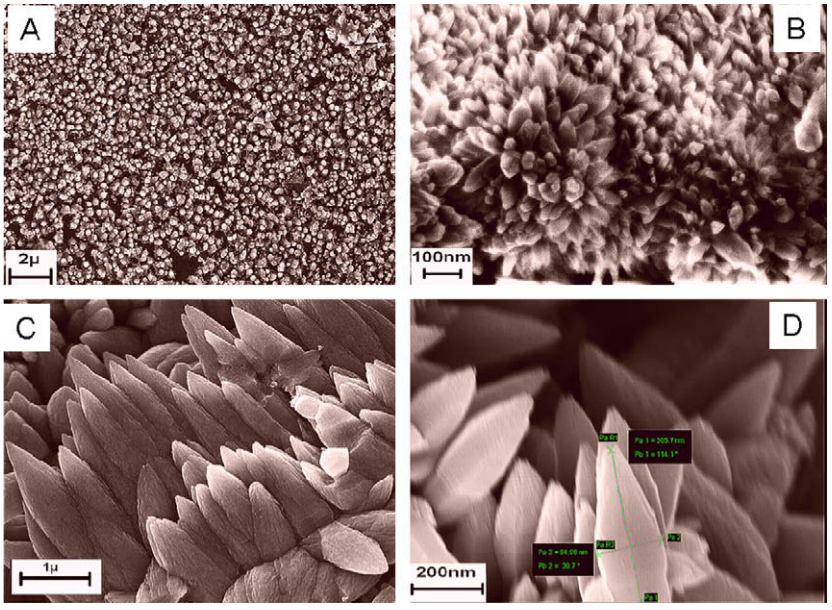

Fig. 6. FESEM micrographs of ZnO nanowires prepared from 0.1 M $Zn(NO_3)6H_2O$ electrolyte at −0.8 V ((A–D) ZnO nanowires at different magnifications).

3.3. X-ray diffraction analysis of aligned ZnO NWs

Fig. 9 shows the X-ray diffractogram of the electrochemically grown ZnO nanowires having lattice parameters $a = 2.93$ Å, $c = 5.45$ Å and wurtzite crystal structure. The crystallites demonstrate an elongation in the [0 0 2] direction and a contraction in the [1 0 0] direction with respect to bulk lattice parameters ($a = 3.24$ Å, $c = 5.20$ Å) [37,38].The intensity of ZnO (1 0 1) reflection remains maximum for all voltages, while the (1 0 0) and (0 0 2) intensities vary with the deposition potential. The relative intensities of the peaks of ZnO were computed considering the highest peak for ZnO i.e. the (1 0 1) peak. The intensity counts for each of the peaks and the calculated relative intensities are tabulated below in Table 1. Therefore, as the deposition potential approaches a more negative magnitude, the preferred orientation of (1 0 1) is deteriorated.

A similar dependence of the preferred orientation of the deposited ZnO films on the deposition potential was previously reported [17]. This is probably because of the presence of Zinc defects in the interstitial voids, causing disordering of the lattice.

The crystallite size of the nanowires estimated from the FWHM (full width at half maximum) values was 22 ± 2 nm for

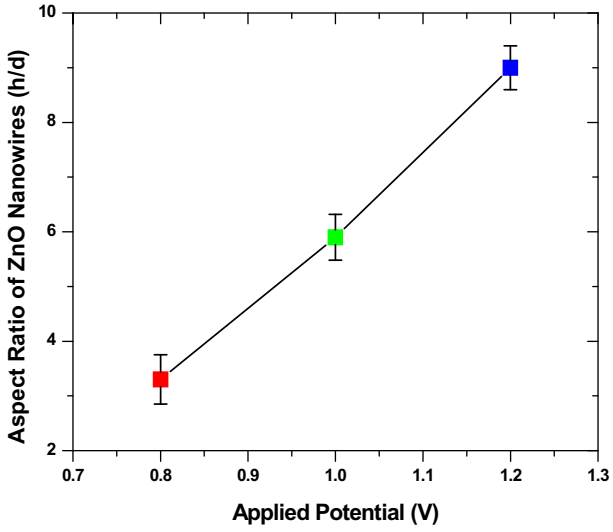

Fig. 7. Variation in aspect ratio of grown ZnO nanowires as a function of deposition potential.

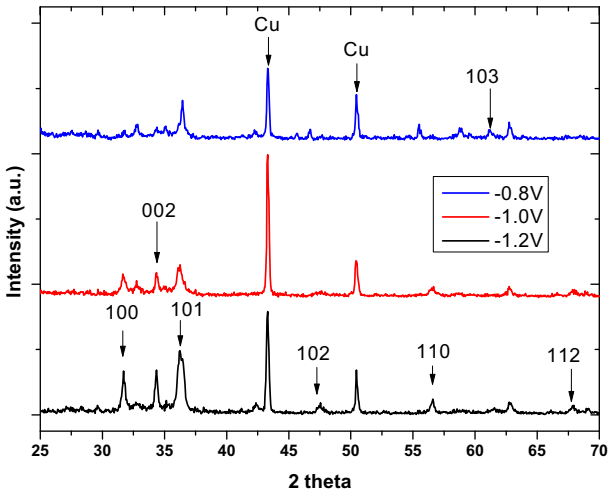

Fig. 9. XRD diffractogram of electrochemically grown ZnO nanowires at −0.8 V, −1.0 V and −1.2 V. XRD measurements were made perpendicular to the growth direction.

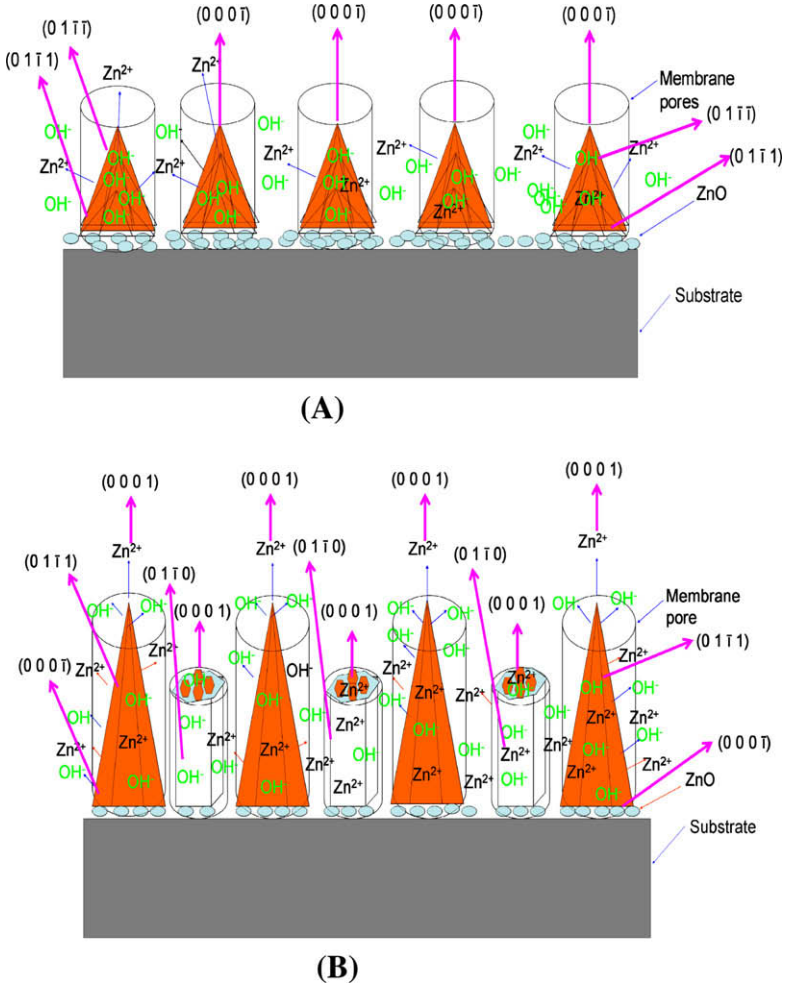

Fig. 8. A and B shows the crystal faces and the mechanism of ZnO growth embedded in polycarbonate membrane.

potentials −0.8 V, −1.0 V and −1.2 V. Considering the relative intensities of the peaks, the crystallite size and diameter from FESEM images, it is possible that the ZnO nanowires are polycrystalline.

3.4. SAXS analysis of aligned ZnO NWs

The crystallite size computed from XRD data is only an average size and the variation with deposition potential cannot be well

Table 1
Intensity counts for ZnO peaks and the calculated relative intensities.

ZnO peak	Intensity (a.u.)	Relative intensity
Case (i) −1.2 V		
(1 0 0)	119	71
(0 0 2)	87	52
(1 0 1)	167	100
Case (ii) −1.0 V		
(1 0 0)	50	27
(0 0 2)	58	31
(1 0 1)	185	100
Case (iii) −0.8 V		
(1 0 0)	42	26
(0 0 2)	42	26
(1 0 1)	161	100

characterized. The estimation of the volume distribution of crystallite sizes in the ZnO nanowires were carried out by small angle X-ray scattering (SAXS) combined with wide angle X-ray diffraction (WAXD. This combination of methods allows us to estimate two relevant size parameters. One of them, derived from SAXS data, gives us information about the size of particles. The other, estimated by WAXD, is the size of crystallites. In the analysis of nanostructure by SAXS, a particle is defined as a volume of homogenous electron density. The definition of crystallite in the analysis of the width of the Debye–Scherrer lines differs from the definition of particle. Generally, a particle can be formed of many crystallites. Although, both methods give weighted average sizes. The scattering intensity $I(q)$ is given by

$$I(q) = \int_{R\min}^{R\max} N(R) I_0(qR) dR \tag{5}$$

I_0 (qR) is the form factor of a sphere of a radius R and $N(R)$ is the density of number of particles as a function of the radius R, in the range between a minimum (R_{min}) and maximum (R_{max}) value.

Fig. 10 shows the variation in SAXS intensities, $I(q)$ versus the modulus of scattering vector, q, in the logarithmic scale for ZnO nanowires deposited at different potentials.

The scattering intensity $I(q)$ maxima computed for ZnO nanowires grown at −1.2 V, −1.0 V and −0.8 V reduction potential are 779, 269 and 130, respectively which indicates a variation in crystallite size distribution. As shown in the graph, the decay of apparent SAXS intensities at larger values of q is significantly faster for ZnO nanowires grown at −1.2 V as compared to the wires grown at −1.0 V and −0.8 V. This result is attributed to the ZnO nanowires subjected at −1.2 V potential having increased fraction of larger crystallites [39]. As the reduction potential approaches to positive side the fraction of large nanostructure crystallites is decreased. When q is low, the decay in scattering intensity, $I(q)$ is not sufficiently different to interpret that the fraction of smaller size crystallites varies with deposition potential. Thus, we can tentatively conclude that the fraction of small crystallites remains the same for the three depositing voltages while the fraction of larger crystallites increases as the potential tends to the more negative side. Hence, the crystallites size computed from the SAXS measurement is ∼20 nm for −1.2 V deposition potential.

3.5. Micro-Raman analysis of aligned ZnO NWs

Fig. 11 shows the Raman spectra of the ZnO nanowires grown at voltages −0.8 V (a), −1.0 V (b) and −1.2 V (c).

The frequencies of the Raman peaks are extracted from experimental data and all the peaks are labeled on the basis of theoretical analysis of symmetry groups as shown in Table 2. In the wurtzite-type ZnO, the high aspect ratio lattice is mainly reflected by two types of lattice phonons. An A_1 branch in which the Raman-active phonon is polarized in the z-direction and an E_1 branch in which the phonon is polarized in the xy-plane are observed. Both A_1 and E_1 symmetries are Raman active and splits into LO (longitudinal optical) and TO (transverse optical) components with different frequencies, because of the macroscopic electronic fields associated with the LO phonons. The lower-frequency E_2 (low) mode is associated with the vibration of the heavy Zn sub-lattice, while the higher-frequency E_2 (high) mode involves only the oxygen atoms within the lattice. Experimentally, E_2 (high) and E_2 (low) phonon modes are observed at 435 cm^{-1} and 96 cm^{-1}, respectively. The FWHM at −0.8 V, −1.0 V and −1.2 V are 49.9, 53.2 and 57.1, respectively. It indicates that as deposition potential approaches to more negative value the FWHM of ZnO nanowires increases, which in turn indicates an increase in number of electron acceptor oxygen atoms in ZnO structure [40].

The broad peak at 328 cm^{-1} is attributed to multiple-phonon scattering processes. An additional weak peak at 206 cm^{-1} is observed and its origin is still not clear. Alim et al. observed a similar peak and suggested that it might be the local vibrational mode related to intrinsic defects in the host lattice [41–43]. However, more

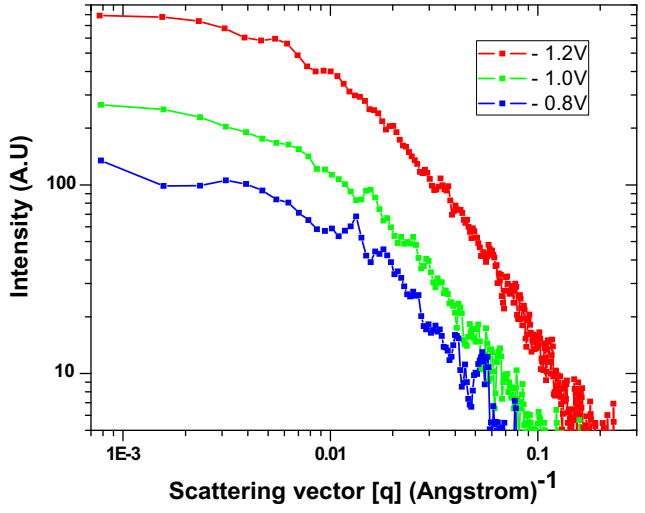

Fig. 10. SAXS intensity $I(q)$ as a function of scattering vector [q] at deposition potentials −0.8 V, −1.0 V and −1.2 V.

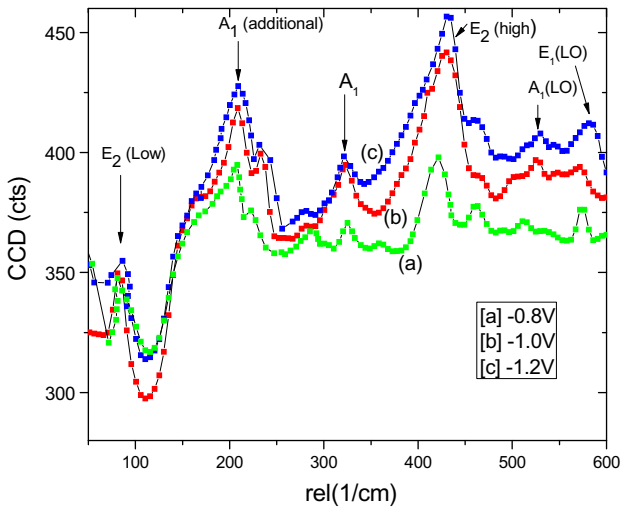

Fig. 11. Micro-Raman scattering spectra of ZnO nanowires grown at voltages −0.8 V (a), −1.0 V (b) and −1.2 V (c).

Table 2
Assignment of Raman peaks on the basis of experimental and theoretical analysis.

Symmetry	Wave number (cm^{-1})			Theoretical Refs. of bulk [41,42]	Nanowire Ref. [2]
	−0.8 V	−1.0 V	−1.2 V		
E_2 (high)	435	437	439	433	438
E_2 (low)	96	98	102	98	–
A_1 (TO)	328	325	329	–	331
A_1 (LO)	542	540	544	548	540
E_1 (LO)	580	584	586	583	584
A_1 (additional)	206	203	205	–	–

research is required to explain this completely [44]. The A_1(LO) and E_1(LO) peaks at 542 cm^{-1} and 580 cm^{-1} are related to smaller scattering cross-sections. They originate from the destructive interference between the Frohlich interaction and the deformation potential contribution to the scattering cross-section of LO phonon in ZnO [45–48]. It is to be noted that the intrinsic defects for oxide materials might be related to Oxygen or Zinc vacancies created during growth. Hence, it indicates that there exist a few Oxygen or Zinc vacancies in wurtzite lattice of the ZnO nanowires.

4. Summary

OSECD is a useful technique for the fabrication of well aligned high aspect ratio ultra thin ZnO NW arrays embedded in polycarbonate membranes. However, the growth of specific orientation, high aspect ratio nanostructures and observation of quantum effects require the appropriate concentrations of the reagents, specific deposition potential and control of NW diameters. A Hot-Probe approach is proposed to characterize the charge carriers available in ZnO nanowires. The SAXS and XRD results show that the ZnO NWs grown at higher negative potential have a higher fraction of larger size crystallites and are polycrystalline in nature. Therefore, OSECD based nanostructures were easily fabricated with added advantages, compared to other techniques. Hitherto unexplored issues of Zinc Oxide nanowires were resolved using innovative characterization techniques and a consequent mechanism of nanostructure growth was proposed.

Acknowledgments

Authors acknowledge the support of the Department of Science and Technology through its IRHPA Grant and the DST Unit on Nanosciences at IIT Kanpur.

References

[1] B.O. Regan, D.T. Schwartz, S.M. Zakeeruddin, M. Gratzel, Adv. Mater. 12 (2000) 1263.
[2] K. Keis, E. Magnussom, H. Lindstrom, S.-E. Lindquist, A. Hagfeldt, Sol. Energy Mater. Sol. Cells 73 (2002) 51.
[3] U. Ozgur, Ya.I. Alivov, C. Liu, A. Teke, M.A. Reshchikov, S. Dogan, V. Avrutin, S.-J. Cho, H. Morkoç, J. Appl. Phys. 98 (2005) 041301.
[4] C.S. Rout, G.U. Kulkarni, C.N. Rao, J. Phys. D. Appl. Phys. 40 (2007) 2777–2782.
[5] D.C. Look, B. Claflin, Phys. Status Solidi B 241 (2004) 624.
[6] B. Pradhan, S.K. Batabyal, A.J. Pal, Sol. Energy Mater. Sol. Cells 91 (2007) 769–773.
[7] T.M. Barnes, J. Leaf, C. Fry, C.A. Wolden, J. Cryst. Growth 274 (2005) 412.
[8] Ju Ko Hang, S.K. Hong, Y. Chen, T. Yao, Thin Solid Films 409 (2002) 153–160.
[9] H.E. Unalan, P. Hiralal, N. Rupesinghe, S. Dalal, W.I. Milne, G.A.J. Amaratunga, Nanotechnology 19 (2008) 255608.
[10] A.B. Hartanto, X. Ning, T.Y. Okada Nakatal, Appl. Phys. A 78 (2004) 299.
[11] S.H. Huang, Zhanghai Chen, X.C. Shen, Z.Q. Zhu, K. Yu, Solid State Commun. 145 (2008) 418.
[12] M. Willander, P. Kalson, L.L. Yang, Safaa-M. Al Hilli, Q.X. Zhao, O. Nur, Phys. Status Solidi (c) 5 (9) (2008) 3076.
[13] D. Gal, G. Hodes, D. Lincot, H.-W. Schock, Thin Solid Films 361 (2000) 79–83.
[14] D. Ramirez, T. Pauporte, H. Gomez, D. Lincot, Phys. Status Solidi (a) 205 (10) (2008) 2371.
[15] J. Leea, Y. Tak, Electrochem. Solid-State Lett. 4 (9) (2001) C63–C65.
[16] Sophie Peulon, Daniel Lincot, J. Electrochem. Soc. 145 (3) (1998) 864–874.
[17] M. Izaki, T. Omi, Appl. Phys. Lett. 68 (17) (1996) 2439.
[18] T. Shinagawa, K. Murase, S. Otomo, J.-i. Katayama, M. Izaki, J. Electrochem. Soc. 156 (5) (2009) H320–H326.
[19] S.K. Volkman, B.A. Mattis, S.E. Molesa, J.B. Lee, A.F. Vornbrock, T. Bakhishev, V. Subramanian, in: IEEE IEDM, 2004.
[20] M.J. Zheng, L.D. Zhang, G.H. Li, W.Z. Shen, Chem. Phys. Lett. 363 (2002) 123–128.
[21] Min Lai, D.J. Riley, Chem. Mater. 18 (2006) 2233–2237.
[22] Jingbia Cui, J. Mater. Sci.: Mater. Electron. (2008) 908.
[23] T. Pauporte, D. Lincot, Appl. Phys. Lett. 89 (2006) 233112.
[24] C.J. Lee, T.J. Lee, S.C. Lyu, Y. Zhang, Appl. Phys. Lett. 81 (2002) 3648.
[25] P.N. Bartlett, S.L. Taylor, J. Electroanal. Chem. 49 (1998) 453.
[26] T. Yoshida, D. Komatsu, N. Shimokawa, H. Minoura, Thin Solid Films 451–452 (2004) 166.
[27] B. Postels, A. Bakin, H.H. Wehmann, M. Suleiman, T. Weimann, P. Hinze, A. Waag, Appl. Phys. A 91 (2008) 595–599.
[28] T.M. Whitney, J.S. Jiang, P.C. Searson, C.L. Chien, Science 261 (5126) (1993) 1316.
[29] J. Elias, R. Zaera-Tena, C. Lévy-Clément, J. Electroanal. Chem. 621 (2008) 171.
[30] Li Wen-Jun, Shi Er-Wei, Zhong Wei-Zhuo, Yin Zhi-Wen, J. Cryst. Growth 203 (186) (1999) 196.
[31] S. Angappane, Neena Susan Johan, G.U. Kulkarni, J. Nanosci. Nanotechnol. 6 (2006) 101–104.
[32] Umair Manzoor, Kyung Do Kim, Physica E 41 (2009) 500.
[33] R. Zaera-Tena, J. Elias, G. Wang, C. Lévy-Clément, J. Phys. Chem. C 111 (2007) 16706.
[34] A. Goux, T. Pauporte, J. Chivot, D. Lincot, Electrochim. Acta 50 (2005) 2239.
[35] D. Das, C.M. Srivastava, D. Bahadur, A.K. Nigam, S.K. Malik, J. Phys. Condens. Matter 16 (2004) 4089–4102.
[36] D.K. Schroder, Semiconductor Material and Device Characterization, John Wiley & Sons, New York, 1998.
[37] R. Maity, S. Das, M.K. Mitra, K.K. Chattopadhyay, Physica E 25 (2005) 605–612.
[38] R. Robert Reeber, J. Appl. Phys. 41 (1970) 5063.
[39] W. Wang, X. Chen, Q. Cai, G. Mo, L.S. Jiang, K. Zhang, Z.J. Chen, Z.H. Wu, W. Pan, Eur. Phys. J. B 65 (2008) 54.
[40] C.N.R. Rao, F.L. Deepak, J. Mater. Chem. 15 (2005) 573–578.
[41] K.A. Alim, V.A. Fonoberov, M. Shamsa, A.A. Balandin, J. Appl. Phys. 97 (2005) 124313.
[42] C. Bundesmann, N. Ashkenov, M. Schubert, D. Spemann, T. Butz, E.M. Kaidashev, M. Lorenz, M. Grundmann, Appl. Phys. Lett. 83 (2003) 1974.
[43] S.C. Shen, M. Cardona, Phys. Rev. B 23 (1981) 5322.
[44] K.A. Alim, V.A. Fonoberov, A.A. Balandin, Appl. Phys. Lett. 86 (2005) 053103.
[45] R. Loudon, Adv. Phys. 13 (1964) 23.
[46] I.P. Kaminow, W.D. Johnston, Phys. Rev. 160 (1967) 19.
[47] M. Tsuboi, A. Wada, J. Chem. Phys. 48 (1968) 2615.
[48] A. Zaoui, W. Sekkal, Phys. Rev. B 66 (2002) 174106.